Mean Velocity and Turbulence Fields Inside a $\beta = 0.50$ Orifice Flowmeter

Gerald L. Morrison, Robert E. DeOtte, Jr., Gregory H. Nail, and David L. Panak
Mechanical Engineering Dept., Texas A&M University, College Station, TX 77843

The flow field inside an orifice flowmeter with a beta ratio of 0.50 operating at a Reynolds number of 91,100 has been studied using a three-color, 3-D laser Doppler anemometer system. Mean velocity measurements show large radial velocities leading into the orifice, the fluid separating from the orifice plate at the throat, the presence of a vena contracta farther downstream, flow reattachment to the pipe wall 5.3 pipe radii (R) downstream, the presence of a small upstream recirculation zone, and both a primary and secondary recirculation zone downstream of the orifice plate. The static wall pressure distribution attains a minimum pressure at 1.5 R, which does not coincide with the location of the vena contracta (0.75 R). Distributions of the entire Reynolds stress tensor are presented along with calculated values of turbulence kinetic energy, turbulence kinetic energy production, vorticity, and turbulence induced accelerations. These data are analyzed to interpret the complex turbulent flow field.

Introduction

Recently questions have arisen about the effect of upstream flow straightener placement upon the discharge coefficient of orifice flowmeters. Work at NIST Boulder (Brennan et al., 1991), NIST Gaithersburg (Mattingly and Yeh, 1991), Southwest Research Institute (Morrow et al., 1991), NOVA HUSKY Research Center (Karnik et al., 1991), and Pacific Gas and Electric Company (Stuart, 1991) have shown that as the flow conditioner is moved along the pipe, the coefficient of discharge begins low when the conditioner (usually a tube bundle) is near the orifice plate. It increases in value passing through the value established by standards and then becoming too large, finally decreases to the correct value as the distance between the tube bundle and the orifice plate becomes very large. All of the studies measured the coefficient of discharge and the flow conditioner location. A few of the studies also measured the mean velocity profile at the upstream flange tap location (usually with the orifice plate removed). It was found that the mean velocity profile varied significantly with the tube bundle location. The question arises as to how much deviation in the mean velocity profile from a "fully developed turbulent pipe flow" can be present before the discharge coefficient varies an unacceptable amount.

One method for answering the question is to continue experimental evaluation until all flow cases have been studied. These experimental programs require significant facility investment and operational expenses but they provide data which are valuable for understanding the mechanism underlying the change in discharge coefficient. However, it is not economically feasible to experimentally determine the discharge coefficient for every flow installation encountered; therefore, the development and validation of a computer program for the numerical prediction of the flow field would be valuable in simulating installation effects. The validation aspect requires significantly more detailed data than is normally collected. What is required is not only the inlet velocity profile and the coefficient of discharge, but detailed distributions of the pressure along the orifice tube wall, the mean velocity distribution throughout the orifice run and information about the turbulence. The last item is required to help analyze the accuracy of the turbulence model used in the numerical simulation.

Texas A&M University, under the sponsorship of the Gas Research Institute, has undertaken the task of providing this detailed experimental database. Through the use of an advanced 3-D laser Doppler anemometer (LDA) system, the mean velocity field and entire Reynolds stress tensor have been measured. This article presents these data along with the calculated quantities; turbulence kinetic energy, vorticity, turbulence production rate and turbulence induced accelerations. This in-

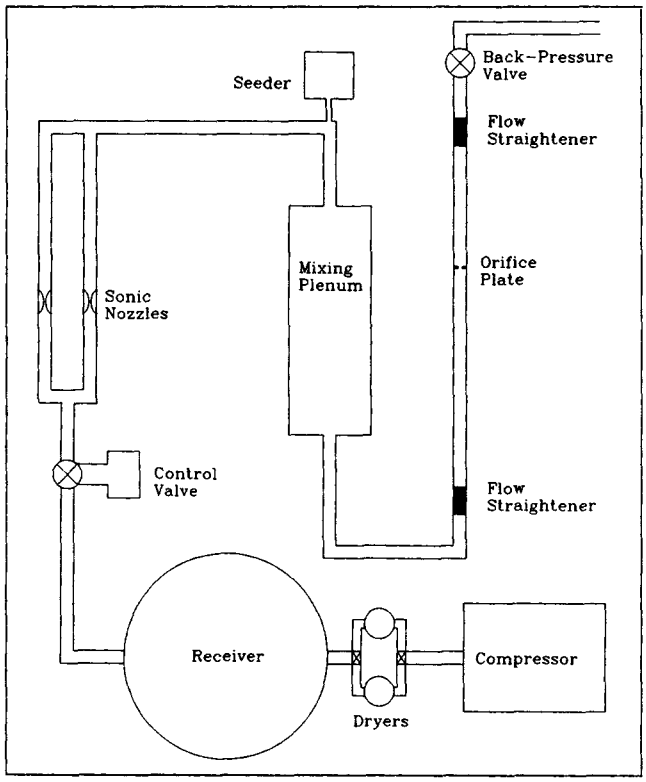

Figure 1. Orifice flowmeter test facility.

formation provides valuable insight into the flow structure present inside the flowmeter as well as providing detailed information for computer code validation.

Background

Morrison et al. (1990a) reviewed the development of the orifice flowmeter and some recent measurements by other investigators (Durst and Wang, 1989; Mittal and Sharma, 1987; Morrison, 1989; Panak, 1990; Patel and Sheikholeslami, 1986; Shen et al., 1988; Teyssandier et al., 1973,1987; and Zedan and Teyssandier, 1986). The conclusion of the literature review is that some hot-wire, 1-D LDA and 2-D LDA measurements have been performed inside orifice flowmeters but none have measured the flow field with a sufficiently fine grid so that spatial derivatives can be calculated for determining turbulence production or vorticity nor have they measured the entire Reynolds stress tensor which is necessary to determine the effects of turbulence upon the mean flow field. This limits the usefulness of the studies for both obtaining an understanding of the complex turbulent flow field present as well as for developing new turbulence models. In addition, the previous studies were typically for a liquid (an incompressible fluid) while the present study was undertaken to provide detailed measurements of the entire flow field inside an orifice flowmeter operating with air (a compressible fluid).

Facilities and Instrumentation

Flow facility

The flow loop used for this study (Figure 1) has been described previously by Morrison et al. (1991b) and DeOtte et al. (1991). Air is supplied by a screw type compressor via desiccant dryers, a large storage tank, an electro-pneumatic pressure regulator, sonic nozzles, a mixing plenum and flow straighteners. The electro-pneumatic pressure regulator is used to maintain the pressure upstream of the sonic nozzles which are operated in a choked flow condition. This maintains a constant flow rate through the orifice flowmeter. The mixing plenum was used to mix the air with atomized "Rosco Fog/Smoke Fluid" which is used for the seed particles that are required for laser Doppler anemometer measurements. Panak (1990) measured the size distribution of the seed and determined that the average size is 0.69 ± 0.5 μm. Daniel 1100F flow straighteners are installed 80 pipe radii upstream and 40 pipe radii downstream of the orifice plate. These distances are approximately twice the distance required by the API 2530 (1985) standard. The presence of the long lengths of pipe and the flow straighteners insures the presence of a swirl free fully developed pipe flow upstream of the orifice plate and prevents the downstream piping from affecting the flow downstream of the orifice plate. A backpressure valve is used to maintain a constant pressure (254 mm Hg, 10 in. Hg) eight pipe radii upstream of the orifice plate. The orifice plate used is a standard orifice plate obtained from Daniel Industries which is 3.175 mm (1/8 in.) thick with a 45° bevel on the last 1.59 mm (1/16 in.) of the plate.

There are two test sections (orifice runs) used in this study. One for the LDA measurements and the other for the pressure measurements. The LDA test section is constructed of acrylic pipe whose side was milled off so as to produce a slit along the length of the pipe (Figure 2). This slit is covered by quartz windows which results in an out of roundness (maximum change in radius compared to the nominal radius) of 1.1%. Measurements performed across the diameter of the pipe resulted in symmetric profiles which indicate that the influence of the window upon the flow field is negligible. The flat window is required so that the six beams of the 3-D LDA remain in alignment as the probe volume is traversed around the flow field. The LDA test section is replaced by the pressure measurement test section for the measurement of the wall pressure distributions along the orifice tube and the orifice plate surfaces. The pressures are measured using a 48 port ScaniValve system, a Validyne pressure transducer and a computerized data acquisition system. The pressures presented are nondimensionalized by the headloss generated by the orifice flowmeter, which is the pressure eight pipe radii upstream of the orifice plate minus the pressure 12 pipe radii downstream.

3-D LDA system

The 3-D LDA system used in this study has been described in detail previously by Morrison (1989), Morrison et al. (1991b), and DeOtte et al. (1991). Briefly the system is a six beam, three color, off-axis backscatter system. An Argon-Ion laser is used to supply three colors: 476, 488 and 514.5 nm. Each color is used to measure an independent velocity component. One optical train is a standard 2-D LDA transmitting system using the 488- and 514.5-nm wavelength light. This optical train is also used to collect the 476-nm scattered light. A second 1-D optical train is used to transmit the 476 nm light and collect the light scattered by the 488- and 514.5-nm light. The axes of the optical trains intersect at a 30° angle. All three colors

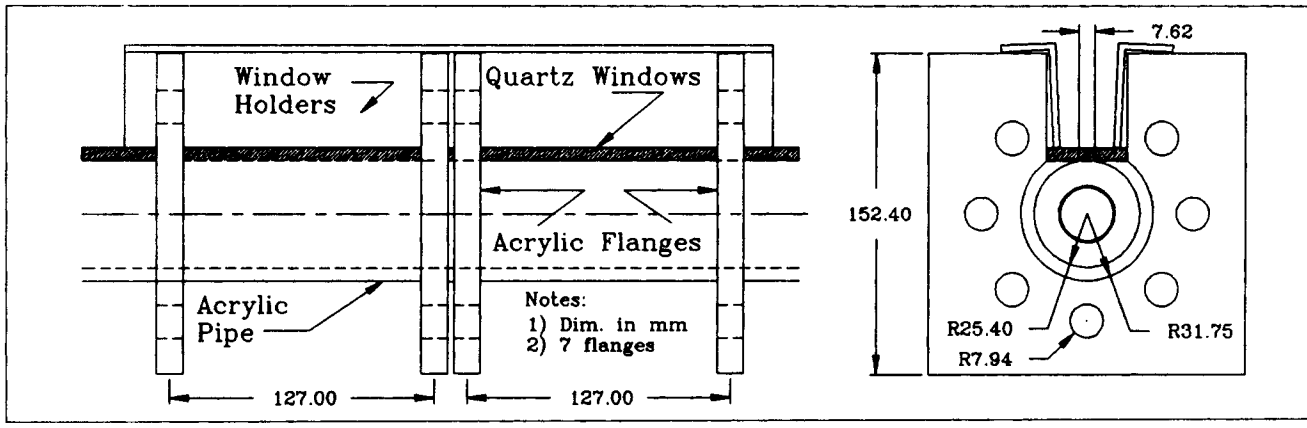

Figure 2. Orifice meter modified for LDA access showing quartz windows and test section construction.

are equipped with Bragg cells to eliminate fringe bias effects and 3.75 × beam expanders to reduce the net probe volume to approximately 0.05 × 0.05 × 0.15 mm (0.002 in. × 0.002 in. × 0.006 in.).

Three instantaneous nonorthogonal velocity components are measured by the three different colored beam sets which are transformed into instantaneous orthogonal velocity vectors. At each spatial location 4,096 instantaneous samples were recorded and used to calculate the mean velocity and Reynolds stress tensor. Inside the recirculation zone downstream of the orifice plate, the local turbulence intensities are very high (exceeding 500%) which results in a velocity bias. The Turbomachinery Laboratory has investigated the velocity bias present in this 3-D LDA system in both free jets (Wiedner, 1988 and DeOtte et al., 1992) and orifice flowmeters (Nail, 1991 and DeOtte et al., 1991). For the free jets statistical averaging, equal time interval sampling, time between data, and the McLaughlin-Tiederman (1973) techniques were evaluated to determine which best met the criteria of conservation of momentum at various axial locations downstream of the nozzle. The present 3-D LDA system has a low sampling rate (100 to 300 samples per second) which results in the statistical averaging, equal time interval sampling, and time between data yielding the same result. The low data rate is characteristic of 3-D LDA systems where the coincidence requirement of the six beams and the arrival time of seed particles greatly reduces the net data rate compared to data rates attainable for each individual color (1,000 to 5,000 samples per second). Only the McLaughlin-Tiederman (1973) method resulted in a meaningful correction for the velocity bias. In the orifice flowmeter only statistical averaging and the McLaughlin-Tiederman techniques were considered. Evaluating the volumetric flow rate at various axial positions resulted in the McLaughlin-Tiederman more closely meeting the requirement of constant volumetric flow rate. Therefore, a full 3-D McLaughlin-Tiederman (1973) correction scheme is used to compensate for velocity bias. This has been discussed in more detail in Nail (1991) and DeOtte et al. (1991).

Morrison et al. (1990b) discussed the errors introduced into the Reynolds stress tensor by the lack of coincidence between the three nonorthogonal velocity measurements and showed that with the nonorthogonal system it is possible to check the quality of coincidence by calculating the correlation coefficient between the nonorthogonal velocity components. They demonstrate that the correlation coefficient for isotropic turbulence is equal to the cosine of the angle between the measured velocity components. This analysis was used to determine the quality of coincidence obtained in this study and to help establish the time coincidence window setting on the counter interface by monitoring the correlation coefficient in the regions upstream of the orifice plate and downstream of the recirculation zone where the turbulence is near isotropic. We established that if this correlation coefficient was low, the resulting LDA measurements contained significant errors, especially in the Reynolds stress terms. For this study a coincidence window of 10 μs was deemed adequate. When all effects are considered the uncertainties on the measured mean velocities are 0.1 m/s and 0.2 m/s on the axial and radial velocities respectively and 0.001 to 0.005 m^2/s^2 for the Reynolds stress components.

Results

Mean velocity field and wall pressure distributions

Velocity measurements were made at approximately 700 locations with 4,096 individual velocity measurements made at each location. The mean values of the velocity for some of these measurements are displayed in the vector field plots in Figures 3 and 4. Additional downstream measurements were made but are not presented. The overall features of the orifice flow field are readily visible in the vector plots. Upstream of the orifice plate, a completely axial velocity profile is evident, typical of that found in fully developed turbulent pipe flow. The appearance of the axial velocity profile in the vector plots is closely allied to that of the empirically obtained "power law" profile as defined in Eq. 1:

$$\frac{u}{U_\ell} = \left(1 - \frac{r}{R}\right)^{\frac{1}{n}} \tag{1}$$

The exponent n varies with Reynolds number. For the Reynolds number of this study n is approximately equal to seven.

As the flow approaches the orifice the velocity vectors exhibit some inward radial turning. The vectors first show signs of radial inward velocity at the $x/R = -1.13$ location. The velocity profiles between this location and the orifice plate show

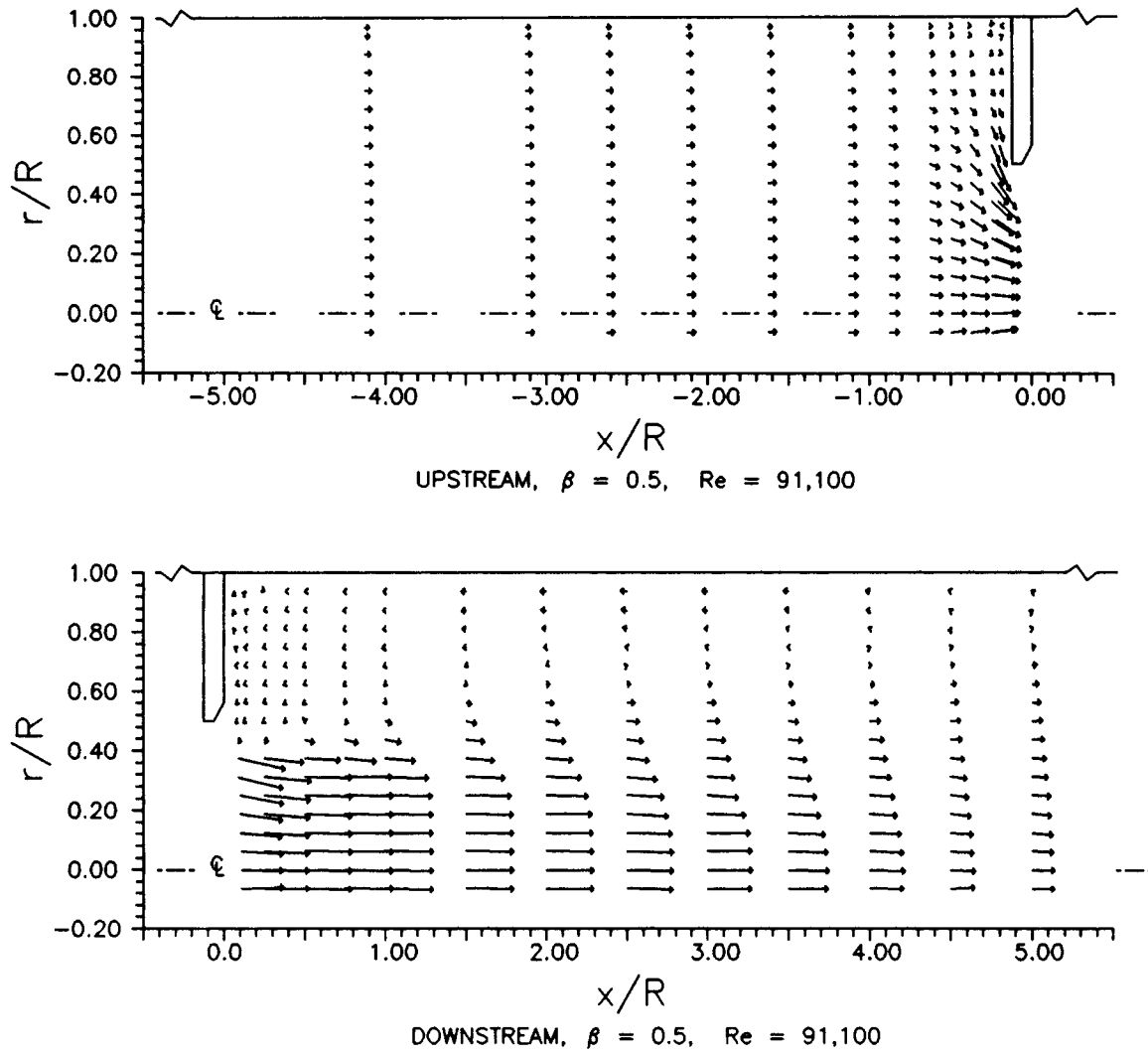

Figure 3. Mean velocity vector field, $\beta = 0.50$, $Re = 91{,}100$.

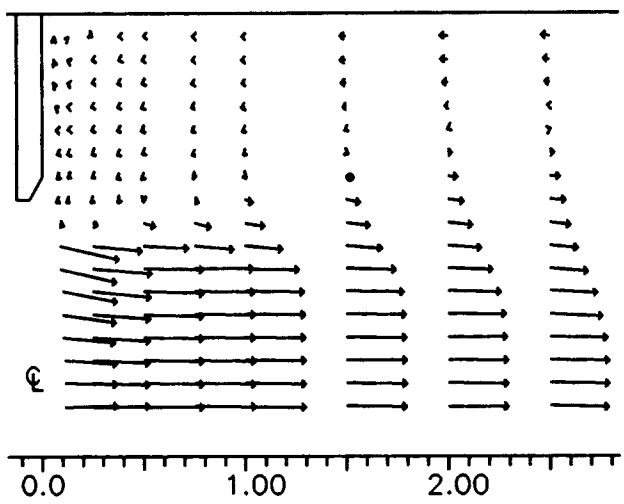

Figure 4. Enlargement of mean velocity vector field in the vicinity of the orifice plate, $\beta = 0.50$, $Re = 91{,}100$.

increasingly larger inward radial velocities. The flow is not able to make the 90° corner at the upstream base of the orifice plate which results in a small recirculation zone being present. In order to accommodate the additional radially inward mass flow, the centerline velocity increases and the centerline flow accelerates axially as it passes through the orifice. This axial acceleration and inward radial momentum increase upstream of the orifice causing the jet to narrow after it issues from the orifice (the vena contracta). A large recirculation zone is present downstream of the orifice with a smaller secondary recirculation zone located at the base of the orifice plate (Figure 4). The jet continues to spread as the flow progresses further downstream resulting in a reattachment of the flow to the pipe wall and eventual redevelopment into a fully developed turbulent pipe flow.

The mean axial velocity distribution along the pipe centerline can be used to identify the location of the vena contracta. This is possible by appealing to the Bernoulli principle and conservation of mass. The vena contracta radially confines the local axial flow (orifice jet) within a relatively small cross-sectional area. There is a corresponding increase in axial ve-

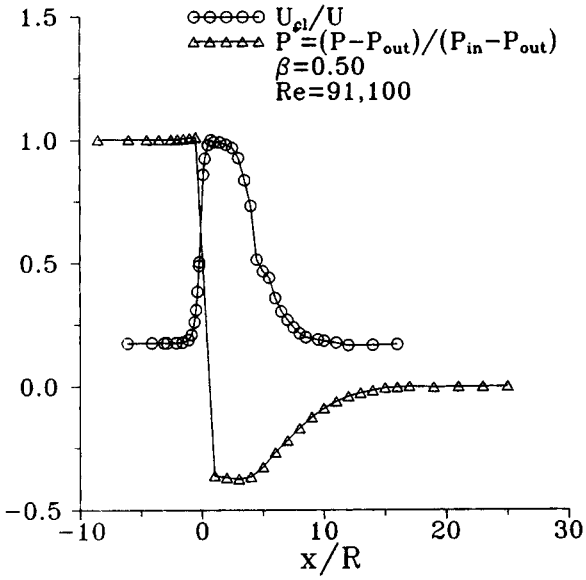

Figure 5. Centerline mean axial velocity and wall pressure axial distributions, $\beta = 0.50$, $Re = 91{,}100$.

locity with the maximum occurring at the narrowest section, which is the vena contracta. Figure 5 shows the centerline distribution of the axial mean velocity overplotted with the mean wall static pressure distribution. The centerline axial velocity begins to increase approximately 1.1 R upstream of the orifice plate, accelerates as it progresses through the orifice, reaches a maximum ($U = 144$ m/s) at 0.75 R, and then, less rapidly decreases during the next 12 radii of flow and begins to approach a fully developed flow again. The tube wall pressure increases very slightly during the last 0.5 R of flow upstream of the orifice plate then decreases rapidly across the orifice plate reaching a minimum of -0.4 at 1.5 R. The pressure then increases as the orifice jet spreads across the pipe reaching its maximum downstream value of 0.0 at 17 R.

It is worthy of note that the axial location of minimum wall pressure is downstream of the maximum centerline mean axial velocity. This phenomena was first reported by Teyssandier and Wilson (1973). It can be explained by recognizing the two-dimensional nature of the pressure field. In order for the minimum wall pressure to occur at the same x/R location as the maximum centerline mean axial velocity, $\partial P/\partial r$ would have to be zero. But the existence of the recirculation zone introduces both axial and radial variations in the velocity and consequently a radially varying pressure field. Therefore the minimum wall pressure and maximum centerline axial velocity are not, in general, expected to occur at the same x/R.

A close examination of the velocity vectors (Figure 4) radially across the jet upstream from the vena contracta reveals that the axial velocity is actually slightly greater nearer the shear layer than on the pipe centerline. This is a direct result of the orifice acting as an obstacle to the flow and forcing the fluid nearer the wall to move radially inward before issuing through the orifice itself. The addition of this mass flow in the center of the pipe causes a corresponding increase in the axial velocity, just downstream of the plate and at the same radial location as the lip. This "overshoot" effect has been previously noted by Durst and Wang (1989).

The gradual spreading and slowing of the jet downstream of the orifice plate is of particular interest. It is important to realize that this feature, while quite similar to a free jet, is also marked by differences. Unlike the free jet, which increases in mass flow because of the entrainment of the surrounding fluid, the pipe orifice jet has no net mass-flow gain or loss. However, the orifice jet spreads out because of an increase in cross-sectional area available to the flow. In addition, the highly turbulent nature of the flow demands that some turbulent exchange of mass take place between the jet and the recirculation zone, but this will result in a net exchange of zero, as in the mean (time averaged) the conservation of mass must be true. The velocity vectors shown in Figure 3 illustrate the large radial velocity imparted to the fluid as it converges toward the centerline to enter the orifice. The mean radial velocity becomes 15% of the maximum centerline velocity just upstream of the orifice along the orifice lip line.

Velocity variance and covariance distributions

The 3-D LDV employed here enabled determination of the complete Reynolds stress tensor. The individual elements of this tensor contain important information about the turbulence occurring in the flow. These quantities are of particular interest to those researchers developing CFD (computational fluid dynamics) techniques with application to turbulent flows. A common approach to turbulence modeling involves the Reynolds (time) averaging of the Navier-Stokes (conservation of momentum) equations. As a result of the Reynolds decomposition and time-averaging process a number of additional terms are generated from the convective acceleration. These terms are of such a form that they are traditionally incorporated into the Reynolds averaged Navier-Stokes equations alongside the shearing stresses, as shown in Eq. 2 for incompressible flow. Thus these terms, six in all (3-D),

$$\rho \frac{D\vec{V}}{Dt} = \rho \vec{g} - \vec{\nabla} p + \mu \nabla^2 \vec{V} - \vec{\nabla} \cdot \vec{\tau}_{\text{turb}} \tag{2}$$

are designated the Reynolds "stresses". Attempts to include the effects of the Reynolds stresses in Eq. 2 constitute turbulence modeling. A common approach is to express them in terms of an empirically derived or evaluated relationship. Knowledge of the actual value of these Reynolds stresses is necessary to ensure that the physics of the turbulence is being realistically incorporated. Knowledge of the Reynolds stress tensor provides information concerning the mechanics of the turbulence that is not otherwise available. This information can also be used in an effort to understand the transport mechanisms due to turbulence.

In 3-D incompressible flows the Reynolds stresses comprise a tensor as shown in Eq. (3). The fact that this matrix is symmetric causes the total number of elements

$$\vec{\tau}_{\text{turb}} = \rho \begin{bmatrix} \overline{u'u'} & \overline{u'v'} & \overline{u'w'} \\ \overline{v'u'} & \overline{v'v'} & \overline{v'w'} \\ \overline{w'u'} & \overline{w'v'} & \overline{w'w'} \end{bmatrix} \tag{3}$$

to be six rather than nine. The terms along the main diagonal represent, in statistical terminology, the variance of the instantaneous velocity components. Similarly, the off-diagonal

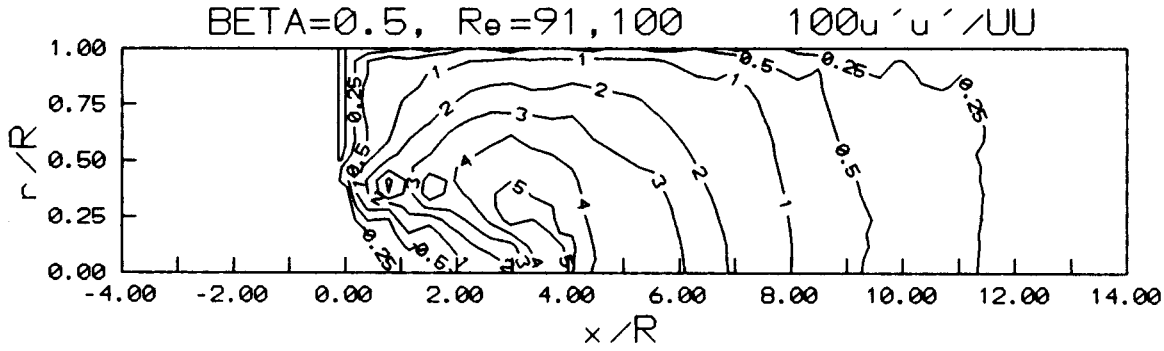

Figure 6. Axial velocity variance, 100 $\overline{u'u'}/U^2$.

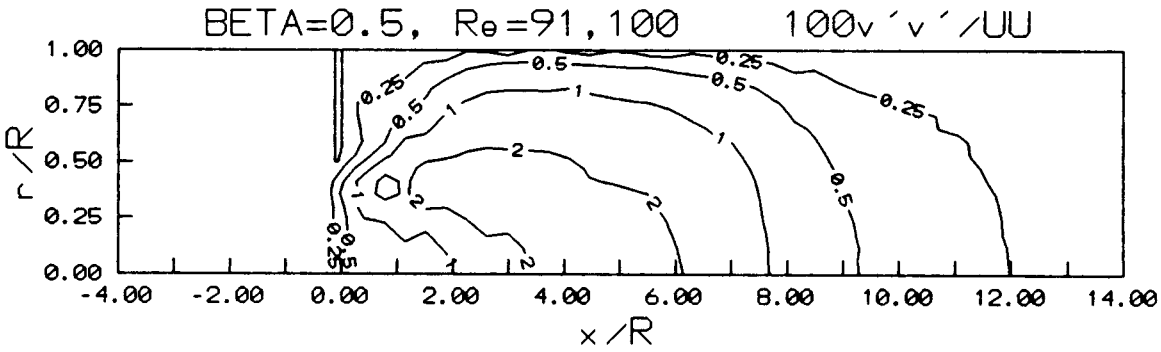

Figure 7. Radial velocity variance, 100 $\overline{v'v'}/U^2$.

terms are actually the covariances. The main diagonal terms are incorporated into the Reynolds-averaged Navier-Stokes equations alongside the normal stresses in such a way as to describe them as "normal" stresses. Likewise, the off-diagonal terms shown in Eq. 3 are incorporated into the Reynolds averaged Navier-Stokes equations so as to be appropriately considered as "shearing" stresses.

The contours of the normal variances are shown Figures 6–8. Each Reynolds stress has been scaled (multiplied) by a factor of 100 and normalized by the square of the maximum axial velocity. The values of each of the variances increases significantly just downstream from the lip of the orifice plate. Figure 3 illustrates the existence of a relatively steep mean velocity gradient in this same area. Initially, the mean velocity gradient is very large which generates small eddies with large levels of vorticity. This is the cause of the rapid rise in the value of turbulence quantities. This region of increasing variances peaks within the shear layer and subsequently decreases gradually in value as the flow progresses downstream. The eddies generated in the shear layer grow in diameter as they radially spread momentum across the shear layer. The radial momentum transfer is the action of the eddies ingesting high speed fluid from the orifice jet and transporting it to the recirculation zone and simultaneously transporting low speed fluid from the recirculation zone into the orifice jet. This action causes the eddies to grow in size, the shear layer to grow in width, and the local time averaged velocity gradient to decrease in value as the flow progresses downstream. The decrease in the local time averaged velocity gradient reduces the energy input of the mean flow into the eddies resulting in the eventual decay of the eddies and hence the turbulence level.

There is little or no increase in the variances upstream of

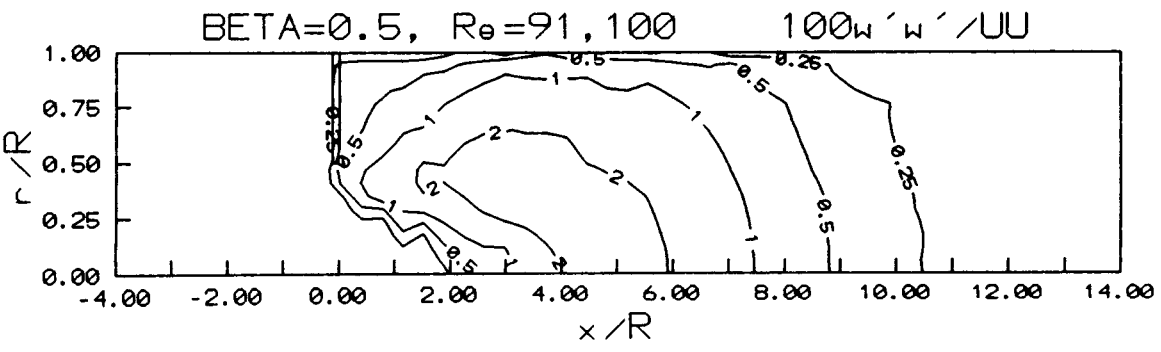

Figure 8. Azimuthal velocity variance, 100 $\overline{w'w'}/U^2$.

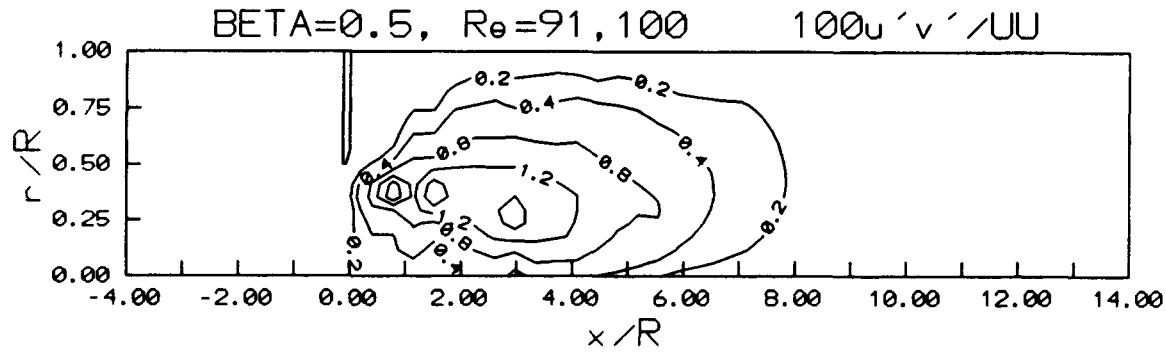

Figure 9. Axial-radial velocity covariance, 100 $\overline{u'v'}/U^2$.

the orifice plate. This is in spite of the presence of mean (radial) velocity gradients there and can be explained on the basis of the simultaneous axial acceleration occurring through the orifice plate, i.e. this acceleration tends to suppress turbulence. In addition, a delay in the onset of the rise in variances can be observed in the vicinity of the jet as it issues through the orifice plate. This effect can be at least partially explained in terms of the suppression of turbulence occurring within the jet itself.

The radial and azimuthal variances are on the order of approximately 50 percent of the corresponding axial value at any given location. This serves as a clear indicator of the anisotropic nature of the turbulence. These results are in general agreement with those previously reported by Shen et al. (1988), Millan et al. (1989) and Durst and Wang (1989). The dominance of the axial variance term has been shown here from the experimental measurements, but was qualitatively anticipated by theory. Tennekes and Lumley (1972) show that in a "pure shear flow" the axial (streamwise) variance receives all of the production of kinetic energy. Therefore, under pure shear flow conditions, the axial variance would be expected to be the only nonzero variance. It follows that the radial and azimuthal variances receive all of their energy via transfer performed by nonlinear pressure-velocity interactions. It is necessary to point out, however, that this analysis was done on an incompressible pure shear flow; therefore, the conclusions reached are valid in an absolute sense only for such cases. One characteristic of the shear flow is the absence of any mean velocity other than axial (streamwise). Also, the only nonzero partial derivative of mean velocity is in the radial direction ($\partial u/\partial r$). Furthermore, the pure shear flow is assumed to have the isotropic dissipative structure characteristic of a high Reynolds number. These assumptions allow for the cancellation of terms and simplifications which permit the previously stated conclusions to be reached. While these assumptions are not exactly met in the case of the orifice run, they are similar enough to explain in a general way the dominance of the axial variance. With reference to shear flows in general Tennekes and Lumley clearly state that typically the axial variance is "roughly twice as large" as the radial and azimuthal variances which is the case for the present measurements.

Contour plots showing the distributions of the three velocity covariances, or off-diagonal (shear stress), terms are presented in Figures 9-11. These off-diagonal elements of the Reynolds stress tensor are measures of the turbulence momentum exchange occurring between the respective velocity component directions. The axial-radial term $\overline{u'v'}$ is an order of magnitude larger than the $\overline{u'w'}$ and $\overline{v'w'}$ covariance terms due to the orientation of the shear layers. The $\overline{u'v'}$ therefore is of prime importance to those researchers developing and evaluating turbulence models. This is because of the traditionally popular scheme of modeling turbulence effects through a turbulent viscosity. The turbulent viscosity, μ_{turb}, has been modeled via various algebraic and other relationships with the axial-radial covariance.

The transport and dissipation processes must be examined in the light of what is happening in the shear layer. The eddies or rollers generated via shearing of the fluid constitute coherent or organized structures which are detected through an increase in the value of the axial-radial covariance. This increase occurs because the eddies have an organized relationship internally between axial and radial velocity components. The axial-radial

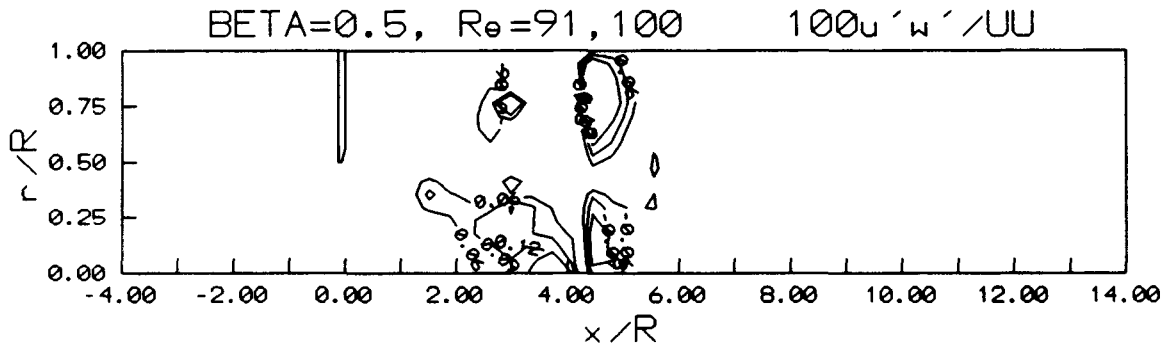

Figure 10. Axial-azimuthal velocity covariance, 100 $\overline{u'w'}/U^2$.

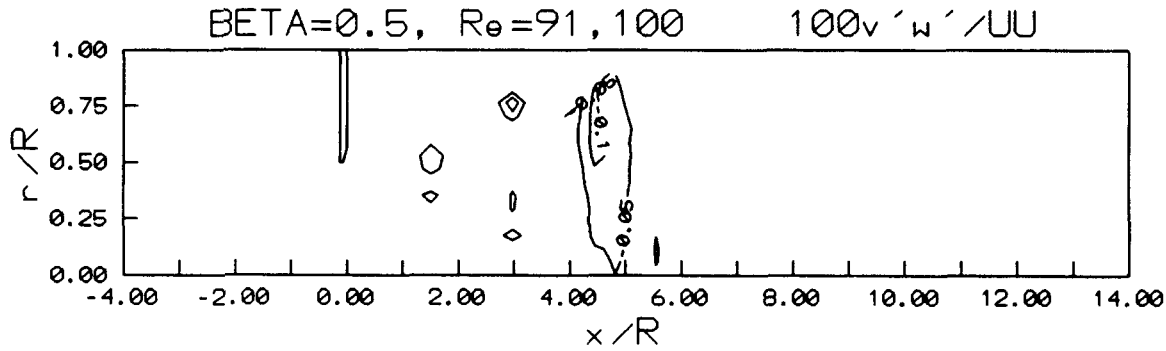

Figure 11. Radial-azimuthal velocity covariance, 100 $\overline{v'w'}/U^2$.

covariance is also a measure of the radial transfer of axial momentum. This phenomena is occurring at the boundary of the shear layer, just downstream of the orifice lip where there is a peak in the values of the covariance. It is in that vicinity that the individual eddies accomplish an exchange of momentum between the slower moving recirculation zone and the high speed orifice jet. The eddies "eject" high speed jet momentum into the recirculation zone while at the same time they "ingest" low speed recirculation fluid into the jet. Therefore, the magnitude of the axial-radial covariance is also a direct measure of the rate of momentum transfer occurring between the recirculation zone and orifice jet via turbulent eddies. It is for these reasons that the distribution of the axial-radial covariance is of importance to turbulence modelers.

The radial-azimuthal and axial-azimuthal covariances for this flow are always less than one-tenth of the axial-radial term which means that the transfer of fluctuating turbulent momentum to the azimuthal direction is negligible. It also means that the fluctuations that do occur are not organized or part of a structure. It must be remembered that this interpretation is predicated on the assumption that the instantaneous velocity components themselves follow a Gaussian distribution. The relatively small value of the radial-azimuthal and axial-azimuthal covariances can and should be accounted for none-theless. In this regard, it is important to recognize that the axial-radial orientation of the shear layer directly contributes to the production of the axial-radial covariance term; consequently the axial-radial covariance ($\overline{u'v'}$) represents eddies generated by the shear layer. Likewise, the absence of any other shear layers means that any other covariance quantity must arise via some mechanism other than shear. An explanation exists when considering the axial-radial eddies generated by the shear layer just downstream of the orifice plate. As they are convected downstream, interaction among and between the eddies cause some straining to occur. As a result, at least some tendency to "wobble" is inevitable. This wobbling will change the orientation of a given eddy from purely axial-radial to some slightly skewed position which will contribute to covariances other than axial-radial ($\overline{u'v'}$); therefore, any wobbling will be detected by the presence of axial-azimuthal ($\overline{u'w'}$) and radial-azimuthal ($\overline{v'w'}$) terms.

Turbulence kinetic energy, turbulence kinetic energy production, and vorticity

The turbulence kinetic energy was computed as defined in Eq. 4, normalized, plotted,

$$\kappa = \frac{1}{2}\left(\overline{u'u'} + \overline{v'v'} + \overline{w'w'}\right) \tag{4}$$

and is shown in Figure 12. This plot shows several general features already covered in the prior discussion concerning Reynolds stresses. A rapid increase in κ can be seen occurring just downstream of the orifice plate tip. Downstream of the peak the contour lines show the widely spaced pattern characteristic of a more gradual dissipation.

The distribution of turbulence kinetic energy is almost identical to that of the individual variances of which it is composed. This is to be expected when taking into account the fact that the distributions of the individual variances are very much alike. Further investigation shows that the distribution of the axial-radial covariance ($\overline{u'v'}$) is nearly the same as that for turbulence kinetic energy. Again this is expected because the

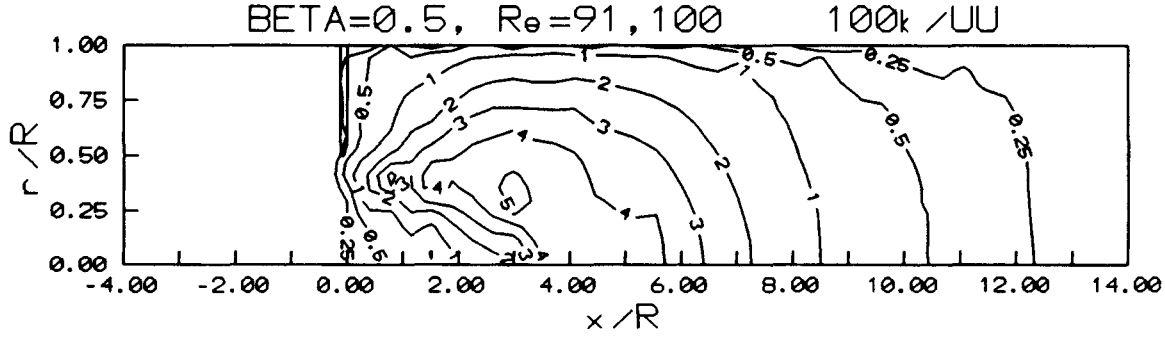

Figure 12. Turbulence kinetic energy, 100κ/U^2.

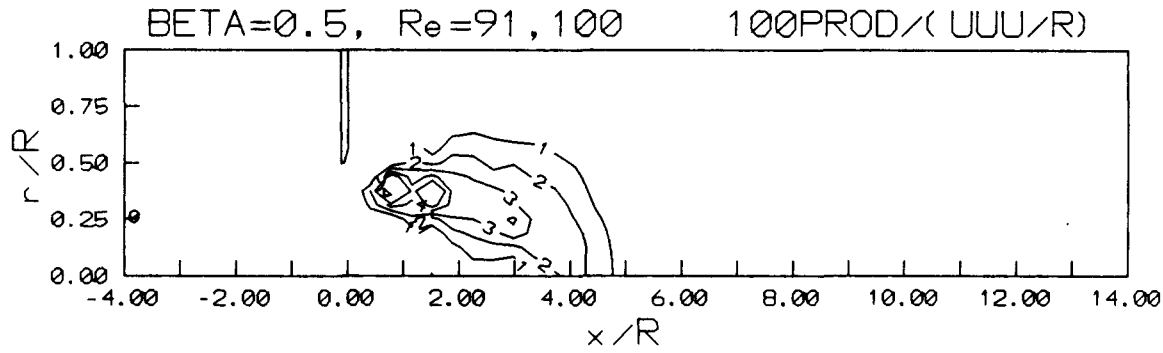

Figure 13. Turbulence kinetic energy production rate, $100E/U^2$.

same phenomena that give rise to the variances also produces the covariance (axial-radial) term.

Turbulence kinetic energy is of primary interest to those researchers developing and evaluating turbulence models. This quantity and especially its spatial distribution is of equal value in verifying numerical models. The results obtained here are generally in agreement with those obtained by Durst and Wang (1989).

The plot of κ shown here also illustrates the processes of production, dissipation, convection and diffusion occurring within the flow. Notice the radial spreading of the contours downstream of the peak. It can be clearly seen that this eventually leads to a more or less uniform distribution of κ across the pipe, by x/R of about 8. After this point κ decays predictably as the flow seeks a return to the fully developed condition. Also evident is a delay in the onset of turbulence inside the jet as it issues from the orifice.

The distribution of the production rate of turbulence kinetic energy (E) is shown in Figure 13. This quantity is defined in Eq. 5.

$$E = -\left(\overline{u'u'}\frac{\partial u}{\partial x} + \overline{u'v'}\frac{\partial v}{\partial x} + \overline{u'v'}\frac{\partial u}{\partial r} + \overline{v'v'}\frac{\partial v}{\partial r}\right) \quad (5)$$

It is evident from Eq. 5 that a region of steep velocity gradients and higher values of Reynolds stresses will likely also be an area of greater E. This situation has already been shown to exist just downstream of the tip of the orifice plate. Figure 13 shows areas of high E just downstream of the orifice plate tip covering a region from $0 \le x/R \le 5$ with the peak production occurring at $x/R \approx 1$. Thus E maximizes while κ is still increasing and has dissipated by the time κ is just beginning to decrease in value.

The mean axial and radial velocity components were used to compute the vorticity of the mean flow. Due to the axisymmetric nature of the flow field there was only one nonzero component of vorticity which is defined in Eq. 6.

$$\Omega_\theta = \left(\frac{\partial v}{\partial x} - \frac{\partial u}{\partial r}\right) \quad (6)$$

Contour plots of the distribution of the azimuthal vorticity defined in Eq. 6 are shown in Figure 14. The vorticity peaks in the vicinity of the tip of the orifice plate. A region of relatively high rate of turbulence kinetic energy production should be expected at or near the same location because of the large mean velocity gradients in that region. The contours near the wall are also expected because of the no-slip condition there. In the near-wall region the axial velocity must undergo a gradient in order to become zero at the wall. It is this $\partial u/\partial r$ quantity that generates vorticity there. This is a mathematical way of stating that the wall causes drag and therefore viscous effects. This same $\partial u/\partial r$ term, when equal to zero, indicates where flow reversal is imminent. (The $\partial v/\partial x$ term is zero anywhere along the wall.) In this way the intersection of the zero contour with the pipe wall is another indicator of the location of a separation or reattachment point.

Notice that the distribution of vorticity is characterized by locally high values just downstream from the lip of the orifice plate. There is a gradual spreading downstream from that location evident via increased spacing between adjacent contour lines. These same general features were observed in the

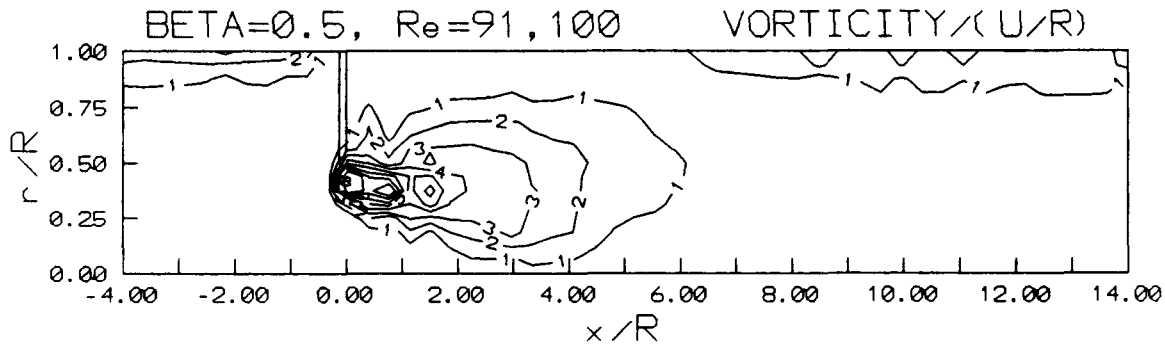

Figure 14. Vorticity, $\Omega R/U$.

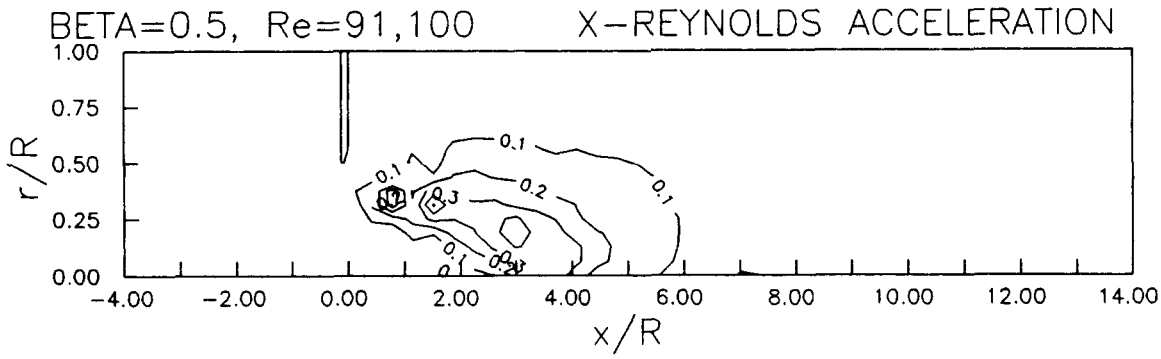

Figure 15. Axial acceleration due to turbulence.

contour plots of the Reynolds stresses. Therefore, the distribution of vorticity throughout the flow field depicts the processes of convective and diffusive transport previously mentioned under the section on the covariant Reynolds stresses.

If a comparison is made between the corresponding plots of κ and E it will be noticed that the areas of peak E *are not* coincident exactly with the areas of maximum κ. A similar observation can be made with regard to the corresponding distributions of vorticity shown in Figure 14. Comparison among the distribution of these three quantities shows the areas of peak E to be most nearly coincident with the areas where vorticity is also a maximum. It is also clear that these areas are where the steepest positive gradients of κ occur. The maximum κ locations are just downstream of the areas of maximum E and vorticity. This observation bears witness to the fact that regions of greater vorticity are also areas of greater entropy production. The location of these regions of maximum E shown here are a confirmation of that conjectured by Shen et al. (1988). They state that, because the turbulence kinetic energy is primarily generated as a result of the actions of the shear layer, the axial-radial covariance distribution should basically correspond to that of the production rate of turbulence kinetic energy. The production rate of turbulence kinetic energy, in conjunction with κ, should be of particular interest to turbulence modelers.

Turbulence induced accelerations

The Reynolds averaged Navier-Stokes equation (Eq. 2) lumps the effects of turbulence into the one term:

$$\vec{\nabla} \cdot \vec{\vec{\tau}}_{turb} \tag{7}$$

Equation 7 actually represents the time-averaged convective acceleration of fluid particles caused by the presence of the turbulence, that is, turbulence induced accelerations. Generally, since the values of the Reynolds stress tensor (Eq. 3) are unknown, it is represented by a scalar, the effective viscosity which is used since the net effect of turbulence is to enhance mixing (momentum transfer) thus increasing the effectiveness of the molecular viscosity in the dissipation of kinetic energy. However, for this study, the Reynolds stress tensor distribution was measured in its entirety and the spatial distribution of the turbulence induced accelerations has been determined.

Figures 15 and 16 present the axial and radial turbulence induced accelerations nondimensionalized by $0.5U^2/R$. Because this is an axisymmetric flow with no swirl, the azimuthal acceleration component is zero. The axial and radial accelerations are nonzero with the axial acceleration being a maximum in the vena contracta region just inside the lipline of the orifice plate. The radial accelerations are positive in the orifice jet region inside the lipline indicating the turbulence is ejecting fluid from the orifice jet into the recirculation zone and causing the jet to spread.

Conclusions

The flow field inside an orifice flowmeter with a beta ratio (β) of 0.50 operating at a Reynolds number of 91,100 has been studied using a three-color, 3-D laser Doppler anemometer system. Mean velocity measurements illustrate large radial ve-

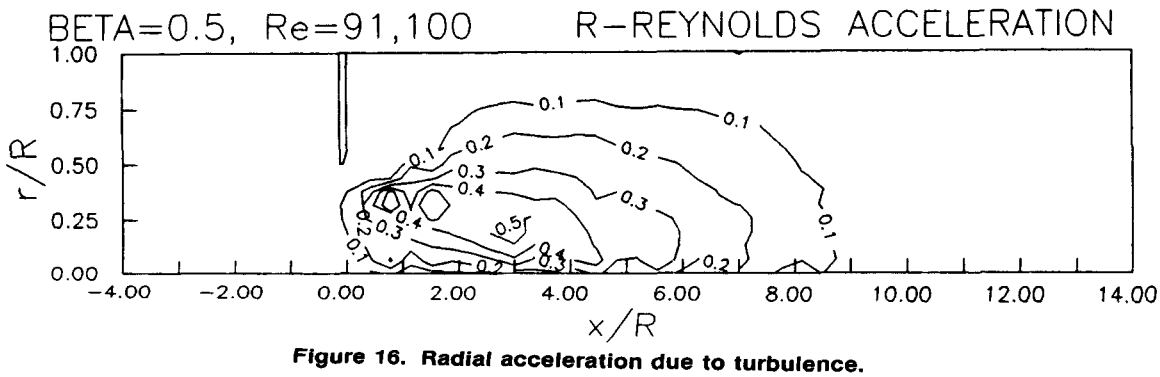

Figure 16. Radial acceleration due to turbulence.

locities leading into the orifice, the fluid separating from the orifice plate at the throat, the presence of a vena contracta farther downstream, flow reattachment to the pipe wall 5.3 pipe radii (R) downstream, the presence of a small upstream recirculation zone and both a primary and secondary recirculation zone downstream of the orifice plate. The static wall pressure distribution attains a minimum pressure at 1.5 R which does not coincide with the location of the vena contracta (0.75 R).

The 3-D LDA system allowed the instantaneous measurement of the entire velocity vector. Hence, the entire Reynolds stress tensor was evaluated at each measurement location. Distributions of the axial, radial and azimuthal variance terms (Reynolds normal stresses) attained maximum values in the shear layer just downstream of the vena contracta. The axial variance term was typically twice as large as the radial and azimuthal variance terms. This is consistent with the turbulence being generated by the one mean velocity gradient ($\partial u/\partial r$). The measured covariance terms show the axial-radial Reynolds stress term being an order of magnitude larger than the axial-azimuthal and radial-azimuthal Reynolds shear stresses. The transport processes of convection and diffusion can be seen on these plots as they show a local peak near the orifice lip which spreads gradually moving in the downstream direction. The structure of turbulent eddies generated by the shear layer was depicted by a contour plot of the axial-radial covariance. A wobbling of the vortex structure was hypothesized as the cause of the existence of some residual axial-azimuthal and radial-azimuthal covariance.

The existence of locally high mean velocity gradients was confirmed by the spatial distribution of the vorticity. The distribution of the axial-radial correlation coefficient confirmed the existence of structured turbulence, especially just downstream from the orifice and in the shear layer. Further attestation to this phenomena was found in the distribution of the radial gradient of the axial-radial covariance. The contours of turbulence kinetic energy and its production rate reflected closely the distribution of the individual Reynolds stress quantities. Significant is the fact that the production rate of turbulence kinetic energy consistently peaked just upstream from the corresponding maximum in turbulence kinetic energy. Turbulence induced accelerations caused the high speed fluid in the orifice jet to mix with the lower speed fluid of the recirculation zone, that is, the turbulence enhanced the radial transfer of axial momentum.

Data Availability

Hard copy and MS/DOS disk listings of the data used in the preparation of this article along with data for $\beta = 0.75$, $Re = 54{,}700$ and $91{,}100$ and $\beta = 0.50$, $Re = 18{,}400$ and $54{,}700$ are available from G. L. Morrison.

Acknowledgments

This work was sponsored by the Gas Research Institute through contract 5086-260-1340 under the auspices of Dr. Max Klein.

Notation

D = orifice pipe (tube) diameter, 50.4 mm
E = turbulent kinetic energy production rate
g = acceleration due to gravity
LDA = Laser Doppler anemometer
P = pressure
P_{in} = inlet pressure measured at $X/R = -8$
P_{out} = exit pressure measured at $X/R = 12$
P^* = nondimensional pressure, $(P - P_{out})/(P_{in} - P_{out})$
Q_o = volumetric flow rate through the pipe
r = radial distance from the pipe centerline
R = pipe radius, $D/2$
Re = Reynolds number, $U_m D/\mu$
u = local mean axial velocity
$\overline{u'u'}$ = mean square of the axial velocity fluctuations (variance)
$\overline{u'v'}$ = mean product value of the axial and radial velocity fluctuations (covariance)
$\overline{u'w'}$ = mean product value of the axial and azimuthal velocity fluctuations (covariance)
U = maximum centerline axial velocity, 144 m/s
U_{cl} = local centerline mean axial velocity
U_m = average mean axial velocity through pipe, $Q_o/(\pi R^2)$
v = local mean radial velocity
$\vec{V}$ = mean velocity vector
$\overline{v'v'}$ = mean square of the radial velocity fluctuations (variance)
$\overline{v'w'}$ = mean product value of the radial and azimuthal velocity fluctuations (covariance)
$\overline{w'w'}$ = mean square of the azimuthal velocity fluctuations (variance)
x = distance downstream from the orifice plate

Greek letters

β = orifice beta ratio, orifice throat diameter/D
θ = azimuthal direction
κ = turbulence kinetic energy, $1/2(\overline{u'u'} + \overline{v'v'} + \overline{w'w'})$
μ = absolute viscosity
ν = kinematic viscosity, μ/ρ
ν_t = eddy viscosity
ρ = density
$\bar{\bar{\tau}}_{turb}$ = Reynolds stress tensor
Ω = vorticity

Literature Cited

Brennan, J. A., C. F. Sindt, M. A. Lewis, and J. L. Scott, "Choosing Flow Conditioners and Their Location for Orifice Flow Measurement," *Flow Measurement and Instrumentation*, **2**(1), 40 (1991).

DeOtte, R. E., Jr., G. L. Morrison, D. L. Panak, and G. H. Nail, "3-D Laser Doppler Anemometry Measurements of the Axisymmetric Flow Field Near an Orifice Plate," *Flow Measurement and Instrumentation*, **2**(2), 115 (1991).

DeOtte, R. E., Jr., G. L. Morrison, and B. G. Wiedner, "Considerations on the Velocity Bias in Laser Doppler Velocimetry," *Sixth International Symposium on Applications of Laser Techniques to Fluid Mechanics*, Instituto Superior Técnico, Lisboa, Portugal (1992).

Durst, F., and A. B. Wang, "Experimental and Numerical Investigations of the Axisymmetric, Turbulent Pipe Flow Over a Wall-Mounted Thin Obstacle," *Seventh Symposium on Turbulent Shear Flows*, Proceedings, **Vol. 1**, pp. 10.4.1-10.4.6, Stanford University (Aug. 21-23, 1989).

Karnik, U., W. M. Jungowski, and K. K. Botros, "Effects of Flow Characteristics Downstream of Elbow/Flow Conditioner on Orifice Meter," presented at the 9th North Sea Flow Measurement Workshop, Bergen, Norway (Oct. 22-24, 1991).

Morrow, T. B., J. T. Park, and R. J. McKee, "Determination of Installation Effects for a 100 mm Orifice Meter Using a Sliding Vane Technique," *Flow Measurement and Instrumentation*, **2**(1), 14 (1991).

Mattingly, G. E., and T. T. Yeh, "Effects of Pipe Elbows and Tube Bundles on Selected Types of Flowmeters," *Flow Measurement and Instrumentation*, **2**(1), 4 (1991).

McLaughlin, D. K., and W. G. Tiederman, "Biasing Correction for Individual Realization of Laser Anemometer Measurements in Turbulent Flows," *The Physics of Fluids*, **16**, 2022 (1973).

Millan, P., P. Gajan, A. Giovannini, A. Alisber, and P. Hebrard, "Basic Study of Flow Metering of Fluids in Pipes Containing an Orifice Plate," Annual Report (May 1988–April 1989), Rept. No: 8/2314/MES, Gas Research Institute (Sept. 1989).

Mittal, R. C., and P. K. Sharma, "Numerical Solution of a Viscous Incompressible Flow Problem Through an Orifice," *Appl. Sci. Research*, **44**, 361 (1987).

Morrison, G. L., "3-D Laser Anemometer Study of Compressible Flow Through Orifice Plates," GRI Report GRI-90/0036 (Nov. 1989).

Morrison, G. L., R. E. DeOtte, Jr., D. L. Panak, and G. H. Nail, "The Flow Fields Inside an Orifice Flow Meter," *Chem. Eng. Prog.*, **86**(7), 75 (July 1990a).

Morrison, G. L., M. C. Johnson, D. L. Swan, and R. E. DeOtte, Jr., "Advantages of Orthogonal and Non-Orthogonal 3-D LDA Systems," *Fifth International Symposium on Applications of Laser Techniques to Fluid Mechanics*, Instituto Superior Técnico, Av. Rovisco Pais, 1096 Lisboa Codex, Portugal (1990b).

Morrison, G. L., M. C. Johnson, and G. B. Tatterson, "3-D Laser Anemometer Measurements in a Labyrinth Seal," *Trans. of the ASME, J. of Eng. for Gas Turbines and Power*, **113**(1), pp. 119–125 (Jan. 1991a).

Morrison, G. L., R. E. DeOtte, Jr., G. H. Nail, and D. L. Panak, "Mean Velocity Field and Turbulence Characterization of the Flow in an Orifice Flow Meter," presented at the Fourth International Conference on Laser Anemometry, Advances and Applications, Cleveland, OH, published in *Laser Anemometry Advances and Applications-1991*, by ASME, A. Dybbs and B. Ghorashi, eds. (Aug. 1991b).

Nail, G. H., "A Study of 3-Dimensional Flow Through Orifice Meters," PhD Dissertation, Texas A&M University (May 1991).

Orifice Metering of Natural Gas and Other Related Hydrocarbon Fluids, 2nd ed., American Gas Association and American Petroleum Institute, ANSI/API 2530 (1985).

Panak, D. L., "3-D Laser Doppler Velocimetry Study of Incompressible Flow Through an Orifice Plate," MS Thesis, Texas A&M University, College Station, TX (May 1990).

Patel, B. R., and Z. Sheikholeslami, "Numerical Modeling of Turbulent Flow Through Orifice Meters," *International Symposium on Fluid Flow Measurement*, Washington, DC (Nov. 1986).

Shen, X., Y. Yan, J. Gao, and Z. Ding, "Turbulent Velocity Measurements in Orifice Pipe Flow with an Improved On-Axis 2-D LDV System," *4th International Symposium on Applications of Laser Anemometry to Fluid Mechanics*, Instituto Superior Técnico, Lisboa, Portugal (July, 1988).

Stuart, John W., Supervising Gas Engineer, Pacific Gas and Electric Company, Private Communication (May 1991).

Tennekes, H., and J. L. Lumley, *A First Course in Turbulence*, 12th ed., The MIT Press, Cambridge, MA and London, England, pp. 74–75 (1972).

Teyssandier, R. G., and Z. D. Husain, "Experimental Investigation of an Orifice Meter Pressure Gradient," *Trans. of the ASME*, **109**, pp. 144–148 (June 1987).

Teyssandier, R. G., and M. P. Wilson, Jr., "The Paradox of the Vena Contracta," *Trans. of the ASME*, Paper 73-WA/FM-9, pp. 1–5 (Dec. 1973).

Wiedner, B. G., "Experimental Investigation of Velocity Biasing in Laser Doppler Anemometry," Thesis for Master of Science, Texas A&M University, College Station, TX (1988).

Zedan, M. F., and Teyssandier, R. G., "Effect of Errors in Pressure Tap Locations on the Discharge Coefficient of a Flange Tapped Orifice Plate," presented at the ASME Winter Annual Meeting, Anaheim, California, 86-WA/FM-3 (Dec. 7–12, 1986).

Manuscript received Aug. 26, 1992, and revision received Nov. 11, 1992.